C. R. Palevol 9 (2010) 349–359

Contents lists available at ScienceDirect

Comptes Rendus Palevol

www.sciencedirect.com

General palaeontology

The inner structural variation of the primate tibial plateau characterized by high-resolution microtomography. Implications for the reconstruction of fossil locomotor behaviours

La variation endo-structurale du plateau tibial chez les primates caractérisée par la microtomographie à haute résolution. Implications dans la reconstruction des comportements locomoteurs fossiles

Arnaud Mazurier[a,*], Masato Nakatsukasa[b], Roberto Macchiarelli[c,d]

[a] *Société Études recherches matériaux, 40, avenue du Recteur-Pineau, 86022 Poitiers cedex, France*
[b] *Laboratory of Physical Anthropology, Graduate School of Science, Kyoto, University Sakyo, Kyoto, Japan*
[c] *Département de préhistoire, UMR 7194, MNHN, 75005 Paris, France*
[d] *Département géosciences, université de Poitiers, 40, avenue du Recteur-Pineau, 86022 Poitiers cedex, France*

ARTICLE INFO

Article history:
Received 8 March 2010
Accepted after revision 30 July 2010
Available online 5 November 2010

Written on invitation of the Editorial Board

Keywords:
Tibial plateau
Inner structure
Locomotor behaviour
Primates
Microtomography
Fossil record

Mots clés :
Plateau tibial
Structure interne
Comportement locomoteur
Primates
Microtomographie
Registre fossile

ABSTRACT

Within the limits imposed by a variety of developmental and rheological constraints, cortical bone adapts to biomechanical loads by partial alteration of its shape, mass and (micro)structure. As bone thickness variation locally reflects the nature, direction, frequency, and magnitude of such loads, some locomotion-related differences are expected in the structural organization of the primate tibial plateau. Here we summarize the results from the first microtomographic-based (SR-μCT) extensive analysis of the topographic variation of the cortico-trabecular complex underlying the adult tibial plateau in a number of primate taxa, including *Homo*. The goals of the study are: (i) to assess the relationships between habitual postural/locomotion-related joint loads and the structural signature recorded by the cortical shell of the articular plateau by comparing the evidence from a bipedally-trained (*Sansuke*) and a wild *Macaca fuscata*; (ii) to assess an "anthropic" (bipedal) pattern; (iii) to explore the possibility to perform similar quantitative analyses on fossil specimens.

RÉSUMÉ

Dans les limites imposées par une variété de contraintes développementales et rhéologiques, l'os cortical s'adapte aux charges biomécaniques par la modification partielle de sa forme, masse et (micro)structure. Puisque la variation d'épaisseur osseuse reflète localement la nature, la direction, la fréquence et l'amplitude de telles charges, des différences liées aux modes de locomotion sont attendues au sein de l'organisation structurale du plateau tibial des primates. Nous résumons ici les résultats de cette première analyse microtomographique (SR-μCT) étendue de la variation topographique du complexe cortico-trabéculaire sous-jacent au plateau tibial adulte de taxons primates, incluant *Homo*. Les objectifs de cette étude sont : (i) d'évaluer les relations entre charges articulaires usuelles

* Corresponding author.
E-mail address: arnaud.mazurier@erm-poitiers.fr (A. Mazurier).

1631-0683/$ – see front matter © 2010 Académie des sciences. Published by Elsevier Masson SAS. All rights reserved.
doi:10.1016/j.crpv.2010.07.020

liées aux comportements posturaux/locomoteurs et la signature structurale enregistrée par l'enveloppe corticale du plateau articulaire, en comparant les résultats extraits d'un *Macaca fuscata* sauvage à ceux d'un cas entraîné à la bipédie (*Sansuke*) ; (ii) d'évaluer le patron « anthropique » (bipède) ; (iii) d'explorer la possibilité de réaliser des analyses quantitatives similaires sur des spécimens fossiles.

1. Introduction

Within the limits imposed by a variety of developmental and rheological constraints, bone tissues respond and adapt to external and internal biomechanical loads by partial alteration of shape, mass, and (micro)structure (Huiskes, 2000; Huiskes et al., 2000; Martin et al., 1998; Odgaard et al., 1997; Ruimerman et al., 2005). As cortical thickness variation and cancellous organization locally reflect the nature, direction, frequency, and magnitude of such loads (Pearson and Lieberman, 2004; Ruff et al., 2006), together with cross-sectional geometric properties, measures of topographic variation of the cortical shell and of trabecular thickness, of bone volume fraction and degree of textural anisotropy (strut number, connectivity density and orientation) can be used as proxy for assessing the taxon-specific dynamic relationships between individual and biomechanical environment (rev. in Volpato, 2008).

While some questions concerning the intimate nature of the functional relationships between the "container" (the cortical shell) and the "contents" (the inner organization) still remain unresolved, the subtle qualitative and quantitative characterization of local morphometric properties of the growing and adult bone allowed the identification of distinct locomotion-related structural features and patterns in selected areas of the human and nonhuman primate skeleton (e.g., Bondioli et al., 2010; Cunningham and Black, 2009; Fajardo et al., 2002, 2007; Gosman and Ketcham, 2008; Jang and Kim, 2010; Link et al., 1998; Macchiarelli et al., 2001a; MacLatchy and Müller, 2002; Maga et al., 2006; Patel and Carlson, 2007; Rafferty, 1998; Ryan and Ketcham, 2002a, 2005; Ryan and Krovitz, 2006; Volpato, 2008). Accordingly, even if the extraction of such endostructural signature in the fossil bone is limited by the usual noise depth resulting from taphonomic dynamics, (in Macchiarelli et al., 2007; Mazurier et al., 2006), these studies are relevant because of their potential application in palaeobiomechanics (e.g., Bondioli et al., 2010; Galik et al., 2004; Lovejoy et al., 2002; Macchiarelli et al., 1999, 2001a; Ohman et al., 1997; Pickford et al., 2002; Rook et al., 1999; Ryan and Ketcham, 2002b; Volpato et al., 2010; Zollikofer and Ponce de León, 2001).

Old World monkeys, apes, and humans display a variety of locomotor and postural modes (Hunt et al., 1996) and their skeletons are characterized by extensive articular size and shape variation at the knee (Ruff, 2002; Tardieu, 1983). Accordingly, because of its functional role of the region involved in body weight transfer to the ground and in the dissipation of the stresses generated by the ground reaction force during locomotion (DeFrate et al., 2004; Freeman and Pinskerova, 2005; Hurwitz et al., 1998), some taxon-related differences are expected in the organization of the subchondral plate of the tibial plateau. However, despite the fact that site-specific bone density and thickness distribution are strong predictors of compressive strength (in Patel and Carlson, 2007), the structural characteristics of this skeletal region remains poorly investigated in a comparative (palaeo)biomechanical perspective, and few quantitative data are currently available on its subchondral compact and trabecular bone density and distribution (e.g., Ahluwalia, 2000; Ding, 2000; Ding and Hvid, 2000; Gosman and Ketcham, 2008; Komistek, 2005; Milz and Putz, 1994; Mockenhaupt and Koebke, 1988, cited by Ahluwalia, 2000; Müller-Gerbl, 1998).

The present study relies upon a quantitative record of the cortico-trabecular complex of the tibial plateau (CTC; see infra) extensively investigated by synchrotron radiation microtomography (SR-μCT) on a human and nonhuman primate sample (Mazurier, 2006). More specifically, its major goals are: (i) to test the extent of the functional relationships between site-specific bone thickness variation and locomotion-related loads at the tibial plateau by quantifying the absolute and relative differences in structural organization found at this site between bipedally-trained and nontrained, wild Japanese macaques (cf. Mazurier et al., 2007). Because of the differences in endostructural bony organization already ascertained at various skeletal sites between bipedally-trained and wild macaques (e.g., Macchiarelli et al., 2001b; Richmond et al., 2005; Volpato et al., 2008), this specific analysis aims to ascertain the degree of reliability and sensitivity of our analytical approach; (ii) to characterize, for future comparative assessment of the bipedal condition in fossil hominins, the "anthropic" pattern, i.e., the pattern typical of the only obligatory biped among the extant hominids, and to compare it to that of *Pan* (cf. Mazurier et al., 2004, 2005); and (iii) to explore the possibility of virtually extracting such endostructural signature from fossil specimens (cf. Mazurier and Macchiarelli, 2006; Mazurier et al., 2006; Volpato et al., 2010).

2. Material and methods

The investigated sample of primate proximal tibiae available in our files consists of 48 adult specimens of both sexes representing the following taxa: *Homo* ($N = 14$), *Pan* (8), *Gorilla* (5), *Pongo* (3), *Hylobates* (3), *Papio* (4), *Theropithecus* (3), *Macaca* (6), *Colobus* (1), and *Pygathrix* (1) (in Mazurier, 2006). Additionally, the sample includes six pathological (4 *Homo* and 2 *Theropithecus*) and two abnormal cases (bipedally-trained *Macaca*). This osteological material comes from the collections of the Muséum national d'histore naturelle (MNHN) and the Musée de l'homme, Paris; the University of Poitiers; the University of Bordeaux 1; the Laboratory of Physical Anthropology,

Kyoto University; the Wake Forest University. The single human fossil specimen investigated so far following the same analytical protocol, i.e., the right tibia La Ferrassie 2, is from a French Neanderthal female skeleton stored at the Musée de l'Homme, Paris (Heim, 1982).

For the specific purposes of the present study, we considered from the sample detailed above: (i) *Sansuke*, a 10 kg adult male *Macaca fuscata* regularly engaged in bipedal performance for eight years, beginning when he was two years old until his death (Nakatsukasa and Hayama, 2003), and, for comparison, the tibia of a nontrained, wild member of the same taxon; (ii) one modern human tibia from a male individual of European origin and that from a *Pan troglodytes* wild female, each displaying the "average" condition of their respective taxon, as illustrated by our currently available record; and (iii) the fossil specimen La Ferrassie 2.

All tibiae have been detailed between 2003 and 2005 by synchrotron radiation microtomography (SR-μCT) at the European Synchrotron Radiation Facility (ESRF) medical beam line ID17, Grenoble. The ESRF microtomographic system, which used a monochromatic beam of nearly parallel geometry and high photon flux associated to a 2048 × 2048 fast-readout, low-noise CCD camera coupled to a fiber-optic taper, leads to a high signal to noise ratio, even on relatively large and fossilized specimens (Mazurier et al., 2006; Pradel et al., 2009; Tafforeau et al., 2006).

Image acquisitions have been performed through 1500 projections during a complete rotation (each 0.24°) using an X-ray beam fixed to 51 keV. Reconstructions of virtual slices were done at the ESRF through an in-house dedicated software (Idltomo), based on a filtered backprojection algorithm. The voxel size of the reconstructed volume is 45.5 × 45.5 × 43.6 μm. Given the average trabecular thickness of the human proximal tibia (167 ± 32 μm; Ding and Hvid, 2000), such a spatial resolution is good enough to provide an accurate rendering of the bony architectural variation beneath the plateau (Mazurier et al., 2006).

Postprocessing of the reconstructed slices consisted in converting the raw data saved in a 32 bit float-format to 8 bit TIFF format. This step was accomplished with ImageJ v1.42 (National Institutes of Health, USA) by adjusting the levels for each stack of slices so that the histogram was evenly distributed within the 256 gray values. Each proximal tibia was then virtually reconstructed in three-dimensions with Avizo 6.1 (Visualization Sciences Group Inc.).

During scanning procedures, the tibiae were positioned with their longitudinal axis perpendicular to the beam axis (i.e., vertically). Although attention has been paid to place each specimen in an anatomical position (i.e., with the articular surfaces parallel to the beam), a virtual transformation of each tibia dataset was necessary to orient all bones in the same way. Each tibia was thus rotated so that both articular surfaces were oriented towards the top of the images. This step has been performed under Avizo 6.1.

We defined the cortico-trabecular complex (CTC) of the tibial plateau as the most dense bony area underlying the articular surface which includes the cortical shell and the intimately related adjoining portions of the supporting trabecular network (plate-like structures). In each investigated proximal tibia, its topographic distribution has been electronically assessed by MPSAK 2.9 (in Dean and Wood, 2003) on virtual parasagittal cross-sections recorded with Avizo 6.1. At regular intervals of 250 μm, CTC thickness has been measured following semiautomatic segmentation along the antero-posterior axis on the medial condyle (MC) and the lateral condyle (LC), perpendicularly to the external bony surface (Fig. 1).

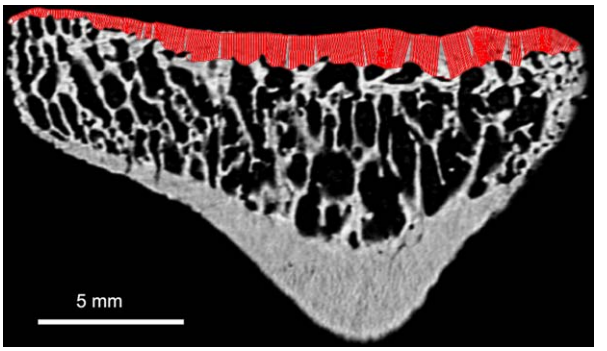

Fig. 1. Example of automated quantification of the cortico-trabecular complex (in red) along the antero-posterior virtual section of the medial tibial condyle of a *Macaca fuscata*. Posterior is left; upper is the articular surface.
Fig. 1. Exemple de quatification automatisée du complexe cortico-trabéculaire (en rouge) le long d'une section virtuelle antéro-postérieure du condyle médial d'un *Macaca fuscata*. Côté postérieur à gauche; la limite supérieure correspond à la surface articulaire.

Repeated intra- and interobserver tests run for accuracy of the measurements provided differences ≤ 5%. Nonetheless, it should be noted that, while our measurement system assures satisfactory accuracy, the assessment of the limits of each condyle is less reliable, as it depends on individual appreciation. Accordingly, besides an estimate of the average thickness variation across its entire extension, we also measured local CTC at five sites corresponding to the anterior, posterior, central, medial, and lateral spots geometrically set within the ellipsoid describing each condyle contour.

In order to quantitatively evaluate the spatial structure and variability of the datasets and to statistically model the degree of heterogeneity of the underground geometry of the CTC, we used the spatial covariance analysis through the variogram function. The variogram is a structure function mostly used in geosciences to describe how local information loses influence with respect to the lag-distance when predicting another local value at another location (Edward and Srivastava, 1989; Gringarten and Deutsch, 2001). An experimental variogram is usually an increasing function of distance, since values of points close together are likely to be more similar than values of far apart points. For a stationary random function, a variogram has three characteristic values: its sill, range, and nugget (Chilès and Delfiner, 1999). At large distance, a variogram may reach a sill, i.e. the ordinate value at which the variogram levels off its asymptotic value, or increase indefinitely (a non-stationary random function with an indefinite mean and/or variance). The sill is an indicator of spatial variability of the data set. The range, or maximum correlation distance, is the distance at which the levelling off occurs, i.e., the

spatial extent of correlation (beyond, data are no longer correlated; in such a case, the most informative portion of a variogram is represented by its shape before the sill). The behaviour near the origin, the nugget, is an important property which reflects the continuity of the variable under study. A discontinuity at the origin, also called the "nugget effect", can be related to either an uncorrelated noise (measurement error) or to spatial structures at a length scale smaller than the minimal distance.

The variogram is also used to interpolate the regionalized variable at points not measured originally. This variogram-based interpolation method, termed "kriging", uses a technique weighting the data in which weights account for the correlation between locations of data pairs and that of the interpolated (Gumiaux et al., 2003).

From the interpolated grid (obtained by Surfer v.8.04, Golden Software Inc.), the CTC distribution and variation is rendered by means of a thickness-related colour map, a simple visualization technique which permits to comparatively appreciate the structural contrasts (e.g., Macchiarelli et al., 2008, 2009).

3. Results

3.1. The morpho-structural test: the bipedally-trained Japanese macaque

According to the *Saru-mawashi*, the tradition of Japanese monkey performance, juvenile male *Macaca fuscata* are trained to acquire an increasingly human-like bipedal gait. The monkeys are exerted to assume an upright bipedal posture and, when they are able to stand stably, they are trained to walk for 2–3 km daily, lasting 30–60 min (Murasaki, 1982).

A number of careful studies have shown to what extent different skeletal sites of the trained macaques adapt to confront the peculiar joint loads and stresses associated with forced bipedal standing and walking (Ogihara et al., 2009). Functionally-related external skeletal changes recorded so far include: lumbar lordosis; increased size of the sacro-iliac and hip joint; postero-proximal extension of the femoral head surface; long axial diameter of the femoral neck relative to the head-neck length; larger knee-joint surfaces; retroflexion and accentuated concavity of the tibial medial condyle (reviewed in Nakatsukasa, 2004; Nakatsukasa et al., 1995). Additionally, structural changes at the cortical level determining increased cross-sectional properties of the long bones (Nakatsukasa and Hayama, 2003) and changes in cancellous patterning involving a higher degree of anisotropy and trabecular re-organization at the ilium and at the proximal and distal femur have been also reported (Macchiarelli et al., 2001b; Richmond et al., 2005; Volpato et al., 2008).

Here, we compare the evidence from a wild specimen to the cortico-trabecular topographic variation of the tibial plateau of *Sansuke*, the macaque engaged in bipedal performance. In *Sansuke*, 387 and 366 measures of CTC thickness have been recorded on the medial and the lateral condyle, respectively; on the tibial plateau of the untrained macaque, these values respectively correspond to 400 and 391 measures.

Table 1
Descriptive statistics and local measures of the cortico-trabecular complex (CTC) thickness at five sites, and surface area and CTC volume of each condyle of the tibial plateau comparatively assessed in a wild *Macaca fuscata* and in the bipedally-trained Japanese macaque *Sansuke*. MC: medial condyle; LC: lateral condyle.

Tableau 1
Statistiques descriptives et mesures locales en cinq points de l'épaisseur du complexe cortico-trabéculaire (CTC), et aire de la surface et volume du CTC de chaque condyle du plateau tibial, évalués comparativement sur un *Macaca fuscata* sauvage et sur un macaque japonais entraîné à la bipédie, *Sansuke*. MC: condyle médial; LC: condyle latéral.

	Wild macaque		*Sansuke*	
	MC	LC	MC	LC
No. of measurements	400	391	387	366
Average thickness (mm)	0.55	0.41	0.80	0.39
s.d.	0.30	0.24	0.37	0.23
Min. thickness (mm)	0.04	0.05	0.12	0.06
Max. thickness (mm)	1.56	1.26	1.96	1.25
Anterior thickness (mm)	0.75	0.40	1.46	0.52
Posterior thickness (mm)	0.79	0.85	0.76	0.36
Central thickness (mm)	0.95	0.62	0.86	0.70
Medial thickness (mm)	0.57	0.50	0.54	0.22
Lateral thickness (mm)	0.76	0.42	0.79	0.21
Articular surface area (mm^2)	167.84	158.84	157.11	152.64
CTC volume (mm^3)	92.10	65.24	125.07	59.52

Distinctly for each condyle, the descriptive statistics and local measures of CTC thickness and the assessment of their respective areas and volumes are shown in Table 1. Compared to the wild macaque, *Sansuke*'s tibial plateau is absolutely and relatively thicker. The medial condyle (MC) is thicker than the lateral one (LC) in both monkeys, but the contrast is much greater in *Sansuke* (51% vs. 25.5%). In both cases, the relative values of the cortical volumes confirm that the medial condyle is more heavily loaded. Here again, *Sansuke* shows the greatest volumetric difference (52.4% vs. 29.2%).

The colour maps, virtually rendering CTC topographic variation in both macaques, are shown in Fig. 2. In the wild macaque, the thickest condylar shell is found near the core of the MC and towards the posterior part of the LC, while thinning concerns the MC's anterior and posterior margins. Along the medio-lateral axis, the inner portion is slightly reinforced compared to the periphery. On the LC, a narrow thicker portion is spread along the antero-posterior axis, with regular anterior thinning.

Sansuke shows a distinct pattern of CTC distribution. Its MC has a major strengthening at the level of the anterior portion of the articular surface, the CTC decreasing posteriorly. With respect to the wild macaque, *Sansuke*'s LC shows a rather homogeneous distribution, being the anterior portion the thickest one. Thickening is distinct in proximity of the spine.

In both specimens, variograms of the medial and lateral condyles are spatially structured at the local and global scale (Fig. 3). Indeed, the shared absence of a nonzero intercept means that the data are smoothly structured when the lag-distance is small (see Mazurier, 2006). Also, the presence of a sill for a finite distance indicates a finite variance, as well as a finite correlation scale. Both macaques show the highest sill for the MC, which means a higher degree

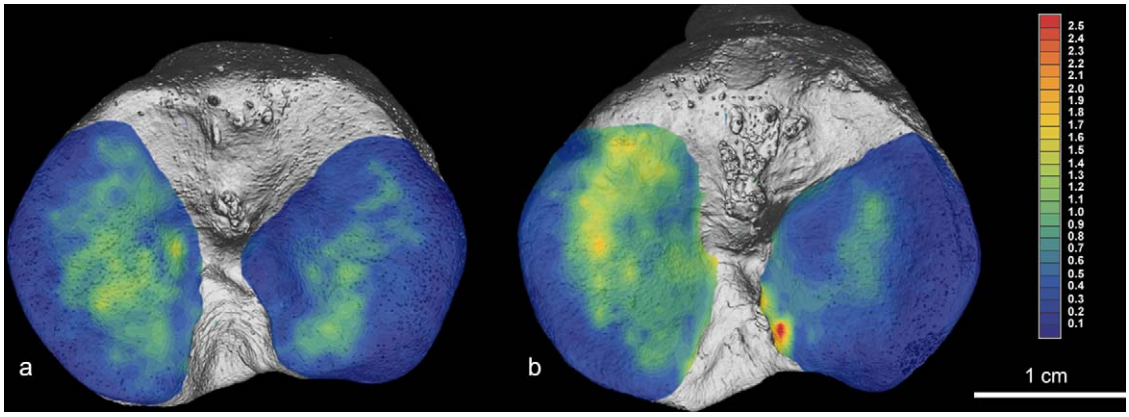

Fig. 2. Microtomographic-based virtual rendering of the local variation of the cortico-trabecular complex thickness of the tibial plateau assessed in: a) a wild *Macaca fuscata*; b) the bipedally-trained Japanese macaque *Sansuke*. Bone topographic variation is rendered by a thickness-related pseudo-colour scale (ranging from "thin" blue to "thick" red). Both tibiae appear as right: medial is left, anterior is upper. *Sansuke* is stored at the Suo Monkey Performance Association, Kumamoto.

Fig. 2. Rendu virtuel, basé sur la microtomographie, de la variation locale de l'épaisseur du complexe cortico-trabéculaire du plateau tibial évaluée chez a) un *Macaca fuscata*; b) le macaque japonais entrainé à la bipédie, *Sansuke*. La variation topographique osseuse est restituée par une échelle de couleur liée à l'épaisseur (variant du bleu « fin » au rouge « épais »). Les deux tibias sont représentés comme des tibias droits: le côté médial est à gauche, le côté antérieur dans la partie supérieure de l'image. *Sansuke* est conservé au Suo Monkey Performance Association, à Kumamoto.

of heterogeneity in the data related to greater thickness. The wild macaque's variograms present a constant increase until a sill. Differently, *Sansuke* systematically shows a rising portion with a "stair" shape. This double sill indicates a couple of nested spatial structures: the first characterized by a smaller correlation length corresponding to the first plateau of variance, which is embedded into a second structure characterized by a larger correlation length corresponding to the second plateau. In *Sansuke*, a small spatial structure can be related to its specific reinforcement of the anterior portion of the articular surface.

As a whole, the unique structural signature revealed by the geostatistical analysis reflects the peculiar nature of *Sansuke*'s locomotor behaviour, having regularly combined for over 8 years the quadrupedalism typical of its taxon to a forced bipedal-like gait. Present results from the inner structural organization of the tibial plateau support previous research on *Sansuke*'s distal femur, showing an increase, likely reflecting stereological loading in bipedal gait, in the degree of cancellous anisotropy through an accentuated sagittal orientation of the trabeculae at the level of the medial condyle (Richmond et al., 2005).

The microtomographic-based 3D reconstruction and virtual animation of *Sansuke*'s right proximal tibia is available at https://nespos-live01.pxpgroup.com.

3.2. The "anthropic" (bipedal) pattern: Homo vs. Pan

The linear, surface, and volumetric measures of the tibial plateau CTC illustrating the "average" (consensus-like) human and chimpanzee condition as represented in our samples (including 14 and 8 specimens, respectively) are shown in Table 2. Compared to *Homo*, *Pan*'s CTC is absolutely and relatively thicker on both condyles, also when

Table 2
Descriptive statistics and local measures of the cortico-trabecular complex (CTC) thickness at five sites, and surface area and CTC volume of each condyle of the tibial plateau comparatively assessed in a modern human adult male (Hs02) and in a wild adult female *Pan troglodytes* (Pt01). MC: medial condyle; LC: lateral condyle.

Tableau 2
Statistiques descriptives et mesures locales en cinq points de l'épaisseur du complexe cortico-trabéculaire (CTC), et aire de la surface et volume du CTC de chaque condyle du plateau tibial, évalués comparativement sur un homme moderne adulte (Hs02) et sur une femelle adulte sauvage de *Pan troglodytes* (Pt01). MC: condyle médial; LC: condyle latéral.

	Homo		*Pan*	
	MC	LC	MC	LC
No. of measurements	2447	2120	1557	1606
Average thickness (mm)	0.54	0.40	0.70	0.56
s.d.	0.48	0.32	0.43	0.47
Min. thickness (mm)	0.03	0.07	0.06	0.05
Max. thickness (mm)	2.39	1.87	1.91	2.53
Anterior thickness (mm)	0.91	0.44	1.02	0.97
Posterior thickness (mm)	0.40	0.82	1.02	0.59
Central thickness (mm)	1.04	0.44	1.02	1.04
Medial thickness (mm)	0.54	0.86	1.03	2.12
Lateral thickness (mm)	1.34	0.30	1.06	0.63
Articular surface area (mm^2)	1211.53	1066.11	707.42	708.07
CTC volume (mm^3)	657.75	428.52	498.36	396.40

scaled to the surface area. In particular, when the ratio average thickness/articular surface area is considered distinctly for each condyle, in the ape tibia the contrast between the medial (1.0‰) and the lateral condyle (0.8‰) is more accentuated than observed in the human specimen represented in this study (0.4‰ in both cases). However, in the African ape the thickest local values are found on the medial aspect of the lateral condyle, while, on average, in the human specimen they concern the lateral aspect of the MC's core.

The human and chimpanzee plateaux share a general model of relative thickening of the cortical shell from the periphery towards the core of each condyle, but in the former this pattern is more marked on the MC, while the opposite is true in *Pan* because of a much less heterogeneous bone distribution across the entire MC's shell. Additionally, *Homo* and *Pan* share a reinforcement towards the intercondylar eminence along the medio-lateral axis of both condyles.

The comparative patterning of CTC topographic variation is rendered by the morphometric maps shown in Fig. 4, resulting from 4567 and 3163 measurements performed on the human and the chimpanzee plateau, respectively. These virtual maps summarize the distinct functionally-related structural signatures distinguishing the human and the ape conditions. In the bent-knee, primarily knuckle-walking quadrupedal *Pan* (Kivel and Schmitt, 2009), a contrast is evident between the sub-rounded thicker spot marking the central portion of the LC (which corresponds to the maximum articular convexity) and the antero-posteriorly rather spread thickening characterizing the MC, reflecting a wider range of motions at the knee-joint typical of the African great apes (Aiello and Dean, 1990; Tardieu, 1983). Conversely, in *Homo*, both thickened areas, notably the medial one, are well-circumscribed and homogeneously surrounded by significantly thinner bone.

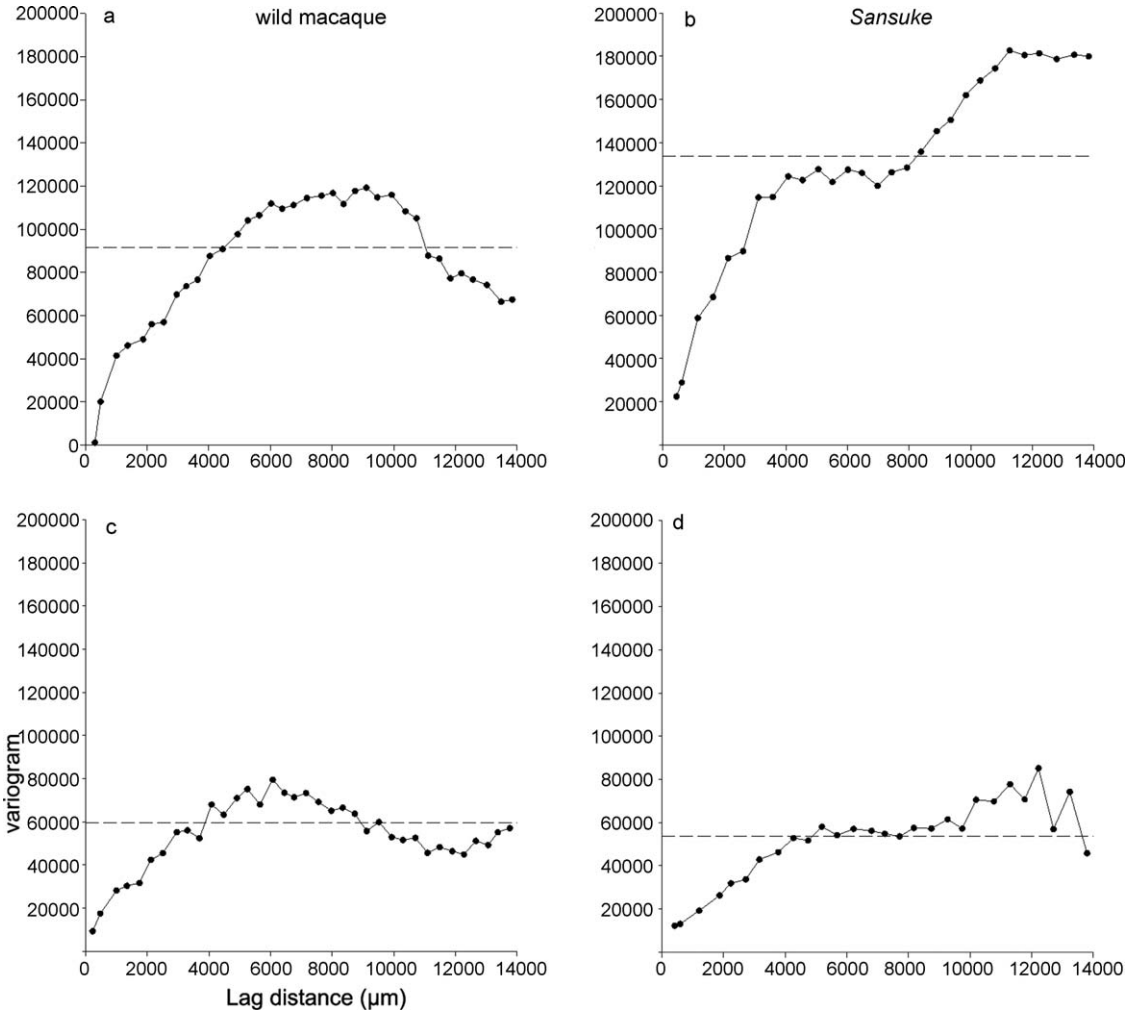

Fig. 3. Variograms calculated for the medial (a-b) and the lateral (c-d) condyles of a wild *Macaca fuscata* (left) and the bipedally-trained *Sansuke* (right). In all cases, the dashed horizontal line represents the global variance in the data. See the text (Material and methods) for methodological details.
Fig. 3. Variogrammes calculés pour les condyles médiaux (a-b) et latéraux (c-d) d'un *Macaca fuscata* sauvage (gauche) et de *Sansuke* entrainé à la bipédie (droite). La ligne noire en pointillés représente la variance globale des données. Voir le texte (section Material and Methods) pour les détails méthodologiques.

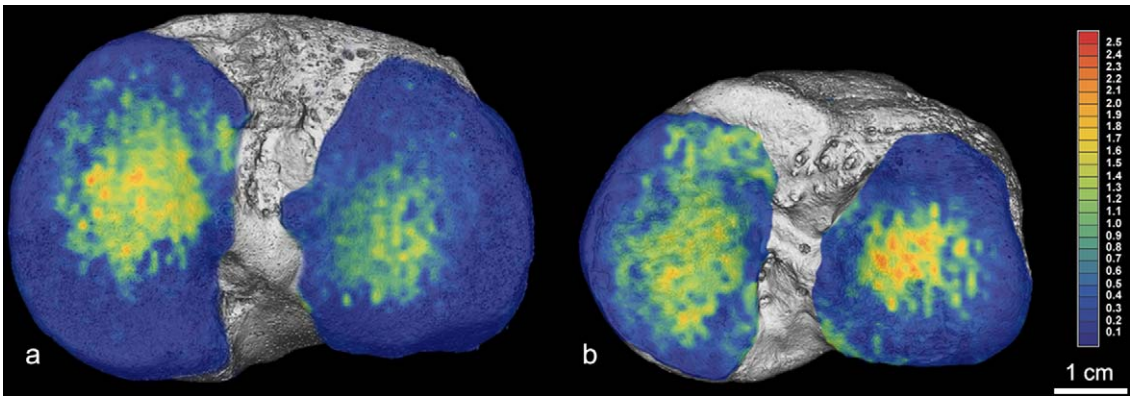

Fig. 4. Microtomographic-based virtual rendering of the local variation of the cortico-trabecular complex thickness of the tibial plateau assessed in: a) a modern human adult male (Hs02); b) a wild adult female *Pan troglodytes* (Pt01). Bone topographic variation is rendered by a thickness-related pseudo-colour scale (ranging from "thin" blue to "thick" red). Both tibiae appear as right: medial is left, anterior is upper.
Fig. 4. Rendu virtuel, basé sur la microtomographie, de la variation locale de l'épaisseur du complexe cortico-trabéculaire du plateau tibial, évaluée chez a) un Homme moderne adulte (Hs02); b) et une femelle adulte sauvage de *Pan troglodytes* (Pt01). La variation topographique osseuse est restituée par une échelle de couleur liée à l'épaisseur (variant du bleu « fin » au rouge « épais »). Les deux tibias sont représentés comme des tibias droits: le côté médial à gauche, le côté antérieur dans la partie supérieure de l'image.

Finally, when the size of the articular surface is taken into account, it is noteworthy that, in comparison to both the wild *Macaca* and *Pan* considered in the present study, *Homo* is characterized by a rather thin cortical shell along the entire surface, locally punctuated by thicker bone on the medial condyle.

While present comparison *Homo vs. Pan* does not rely upon a conclusive statistical analysis but on the evidence extracted from a single "average" individual representative of each taxon, it clearly illustrates the nature and extent of the locomotion-related structural differences imprinted in the mammalian skeleton at the level of the tibial plateau and their potential value in comparative biomechanics.

3.3. The fossil perspective

To the best of our knowledge, besides the Neanderthal specimen La Ferrassie 2 considered in the present study, no fossil primate tibia has been detailed by high-resolution microtomography and reported so far for the subtle organization and site-specific variation of its subchondral proximal plate, the left tibia Spy 9 from another adult Neanderthal skeleton from Belgium having been recorded by medical CT at a voxel size of $209 \times 209 \times 300\ \mu m$ (Volpato et al., 2010).

The 3D surface reconstruction of La Ferrassie 2 tibial plateau (upper view) and the 1 mm-thick virtual coronal section running through the middle of its proximal end are shown in Figs. 5 a and b, respectively. Despite the taphonomic history experienced by this ca. 50 000 year old human fossil bone and the restoring interventions having locally deeply affected its inner structure (as shown by the large white spots appearing on the medial portion of the epiphysis imaged in Fig. 5b), the preservation quality of its subchondral compact bone and the adjoining portions of the rod- and plate-like structures forming its cancellous network are, as a whole, finely preserved, and allow a reliable quantification of their topographic variation across most of the articular surface.

Compared to the modern human condition, Neanderthal long bones show significantly thickened cortical tissue and medullary narrowing (e.g., Churchill, 1998), resulting from greater bone deposition on the endosteal rather than periosteal surface. Our analysis of the La Ferrassie 2 upper end clearly shows that, in Neanderthals, not only the tibial shaft is absolutely thicker (Trinkaus and Ruff, 1999; Volpato et al., 2010), but also the articular plateau, the thickest value of 3.16 mm having been recorded on its lateral condyle. Similar to the pattern shown by the modern human reference specimen (Table 2, Fig. 4a), also in La Ferrassie 2 the contrast between the thicker MC (average: 1.19 mm) and the thinner LC (0.86 mm), is quite marked; additionally, within each condyle, here also the thicker central spot is surrounded by significantly thinner bone.

While detailed at significantly different resolutions, the tibial plateaux of the two adult Neanderthal skeletons La Ferrassie 2 and Spy 9 show a similar organizational pattern. However, the cortico-trabecular thickness recorded on Spy 9 is, on average, 3 mm thicker (Mazurier, 2006), an evidence suggesting more strenuous levels of physical activity experienced by this latter individual, and/or sex-related variation (Volpato et al., 2010).

The most striking evidence resulting from our preliminary analysis of La Ferrassie 2's proximal tibia likely concerns the structural patterning of the trabecular network immediately beneath the cortical shell, which shows an important number of parallel thickened struts obliquely running from the centre of the articulation towards the medial condyle (Fig. 5b). Also, besides the evidence from our own comparative modern sample, in the Neanderthal specimen the average thickness of the sub-epiphyseal trabeculae exceeds the estimates provided by Gosman and Ketcham, 2008; see Table 1 and Fig. 2E) on a late prehistoric human skeletal sample from the Ohio Valley.

The microtomographic-based 2-3D reconstruction and virtual animation of the upper end of La Ferrassie 2's right tibia is available at https://nespos-live01.pxpgroup.com.

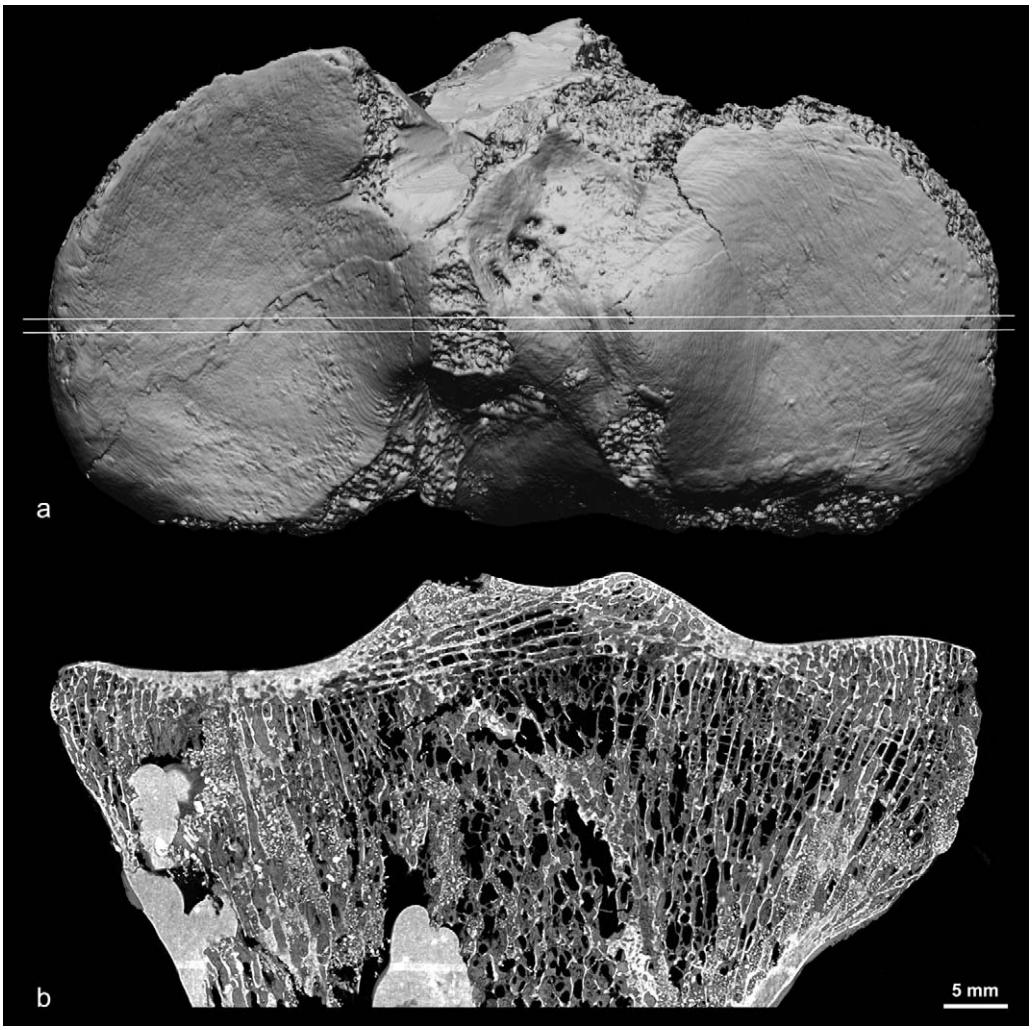

Fig. 5. The right tibia from the adult female Neanderthal skeleton La Ferrassie 2. a) microtomographic-based 3D reconstruction of the proximal end in upper view, with indication of the 1 mm-thick virtual coronal section; b) 3D rendering of the virtual coronal section set in the image shown above. The white spots appearing to the left correspond to restoring interventions. In both images, medial is left. The original fossil specimen is stored at the Musée de l'Homme, Paris.

Fig. 5. Le tibia droit du squelette d'une femme adulte de Néanderthal, La Ferrassie 2. a) reconstruction 3D, basée sur la microtomographie, de l'épiphyse proximale en vue supérieure, avec indication de la position d'une section coronale virtuelle de 1 mm d'épaisseur; b) rendu 3D de la section coronale virtuelle présentée ci-dessus. Les taches blanches visibles à gauche correspondent à des interventions de restauration. Pour les deux images, le côté médial est à gauche. Le spécimen fossile original est conservé au Musée de l'Homme, Paris.

4. Discussion and concluding remarks

Comparative functional anatomy shows that the mammalian knee is "an alarmingly complex joint" (Lovejoy, 2007: p. 326), and that the morphologies of the distal femur and proximal tibia are deeply conditioned by their specific function within a biomechanical unit.

Because of their wide range of postural and locomotor modes, important variation exists among primates in size and shape of the medial and lateral articular surfaces and the intercondylar tubercles of the tibial plateau (Tardieu, 1983). This reflects functional adaptation to a variety of biomechanical constraints related to the direction, magnitude, and frequency of the loads at the knee-joint (Aiello and Dean, 1990). Nonetheless, while external functional variation has been reported, much less is known about the subtle inner structural morphology of this joint.

A remarkable attempt to examine the correlation among locomotor behaviour, gross articular morphology of the knee, and bone density/structure of the subchondral bone of the tibial plateau in a number of catarrhines is due to Ahluwalia (2000). According to her results, an examination of the proximal tibia alone can be enough to assess the mediolateral loading patterns. More precisely, mediolateral differences in loading of terrestrial catarrhines knees, which are reflected in morphological and density adaptations of the condyles to increased load on the medial side of the knee, can be predicted based on differences in hindlimb geometry and locomotor behaviour (Ahluwalia, 2000). Also, similarly to our results, Ahluwalia's

study showed that, with respect to a leaping arboreal quadruped, the loading-related subchondral bone density pattern characteristic of bipeds, knuckle-walkers, and terrestrial monkeys is greater on the medial side of the knee and that the discrepancy in loading between the two sides of this joint, favouring the medial side, is greatest in the knuckle-walking great apes.

However, despite the value of this pioneering investigation, the resolution of her 1–2 mm-thick tomographic-based record does not allow a fully satisfactory rendering of the density contour maps of the 142 investigated proximal tibiae, notably of the typical human condition. Conversely, based on our research experience on the qualitative and quantitative characterization of cortical and trabecular bone structural variation and local properties in modern and fossil specimens (e.g., Bondioli et al., 2010; Mazurier, 2006; Mazurier et al., 2006; Volpato et al., 2010), high-resolution microtomography represents the best investigative tool currently available for the 3D imaging and noninvasive assessment of bony conformation patterns. When the specific needs and constraints of the present (paleo)biomechanical investigation are considered, the system set at the ESRF ID 17 beamline used in our analyses likely represents the best compromise between spatial resolution, which is enough to carefully detail individual strut size, and average size of the proximal tibia in human and nonhuman primates, including large-bodied apes.

With special reference to the three main goals of our study, present results show that:

(1) an intimate relationship exists between site-specific bone thickness variation at the tibial plateau and locomotion-related functional loads at the knee-joint. In fact, compared to the typical pattern evidenced by a wild *Macaca fuscata*, the test-case represented by the skeleton of the bipedally-trained *Sansuke* unequivocally demonstrates a thicker cortico-trabecular complex (CTC), particularly accentuated at the level of the medial condyle. This suggests a more pronounced adducted moment during the forced bipedal-like locomotion, which can result from the more laterally oriented hip and knee joints (Hirasaki et al., 2004; Ogihara et al., 2009). Additionally, the anterior reinforcement of the tibial plateau likely plays an important role in the absorption and dissipation of loads related to a more extended hindlimb joint and the use of an inverted pendulum-like mechanics during bipedal locomotion (Hirasaki et al., 2004);

(2) the three-dimensional "anthropic" pattern revealed by our high-resolution quantification of the CTC topographic variation, which unequivocally distinguishes *Homo* from *Pan*, fits the expectations resulting from a variety of previous analytical approaches to the assessment of the human tibial plateau inner structure (e.g., Ding et al., 2002; Milz and Putz, 1994; Mockenhaupt and Koebke, 1988; Müller-Gerbl, 1998). Also, our model permits us to refine the low-resolution-based evidence provided by Ahluwalia (2000) and to quantitatively show that, when scaled to the articular surface area, the human CTC is significantly thinner at both condyles than that of *Macaca* and, to a lesser extent, of *Pan*. However, the nature of such inter-taxic differences in cortical bone thickness (volume) variation, likely reflecting the influence of functional as well as metabolic factors, deserves additional investigation. In *Homo*, load distribution at the tibial plateau increases from the periphery of the articulation towards the intercondylar spine (Mow et al., 1992) and, compared to the chimpanzee condition, the relatively thicker medial condyle reflects maximal strength centrally and slightly anteriorly (cf. Ding et al., 2002) because of an adduction moment typical of the knee-joint kinematics associated to the bipedal gait (Freeman and Pinskerova, 2005; Hurwitz et al., 1998; Iwaki et al., 2000; Johal et al., 2005). Of course, aspects concerning population-, age-, and sex-related structural variation at this skeletal site still deserve extensive research on human and nonhuman primates;

(3) finally, combined with the assessment of an "anthropic" reference pattern, the successful high-resolution imaging and preliminary quantitative characterization of the endostructural signature virtually extracted from the proximal end of a fossil human tibia (the Neanderthal specimen La Ferrassie 2) confirm the reliability and accuracy of the microtomographic-based analytical approach and, in our view, open new potential perspectives in the study of the hominid fossil record.

Acknowledgements

We are very grateful to G. Clément and D. Geffard-Kuriyama for their kind invitation to contribute this special number on 3D imaging. We are indebted to the Suo Monkey Performance Association, Kyoto, for permission to study the bones of *Sansuke*, to the MNHN, Paris, for access to the primate osteological collection (courtesy of C. Lefèvre), and to the Musée de l'Homme, Paris, for access to the anthropological collection and to the Neanderthal tibia La Ferrassie 2 (courtesy of P. Mennecier). For discussion on this project, we thank L. Bondioli, J. Braga, F. Delay, B. Maureille, P. Semal, L. Rook, V. Volpato, A. Walker, and D.S. Weaver. The comments from two anonymous reviewers significantly enhanced the quality of the earlier version of the present paper. A. Bravin, C. Nemoz, and P. Tafforeau provided a valuable contribution during acquisitions at the ESRF, Grenoble. For technical collaboration and supplementary acquisitions and elaborations, we also acknowledge the Centre de Microtomographie at the Univ. of Poitiers (P. Sardini). Research supported by the CNRS, the ESRF, the GDR 2152, the Région Poitou-Charentes, the Nespos Society, the Univ. of Poitiers.

References

Ahluwalia, K., 2000. Knee joint load as determined by tibial subchondral bone density: its relationship to gross morphology and locomotor behavior in catarrhines. PhD Thesis, State University of New York, Stony Brook, 315 p.

Aiello, L., Dean, C., 1990. An introduction to human evolutionary anatomy. Academic Press, London, 608 p.

Bondioli, L., Bayle, P., Dean, M.C., Mazurier, A., Puymerail, L., Ruff, C., Stock, J.T., Volpato, V., Zanolli, C., Macchiarelli, R., 2010. Morphometric maps of long bone shafts and dental roots for imaging topographic thickness variation. Am. J. Phys. Anthropol. 142, 328–334.

Chilès, J.-P., Delfiner, P., 1999. Geostatistics: modelling spatial uncertainty. Wiley Inter-Science, New York, 695 p.

Churchill, S.E., 1998. Cold adaptation, heterochrony, and Neandertals. Evol. Anthropol. 7, 46–61.

Cunningham, C.A., Black, S.M., 2009. Anticipating bipedalism: trabecular organization in the newborn ilium. J. Anat. 214, 817–829.

Dean, M.C., Wood, B., 2003. A digital radiographic atlas of great apes skull and dentition. In: Bondioli, L., Macchiarelli, R. (Eds.), Digital Archives of Human Paleobiology. ADS Solutions, Milan (CD-ROM).

DeFrate, L.E., Suna, H., Gilla, T.J., Rubasha, H.E., Li, G., 2004. In vivo tibiofemoral contact analysis using 3D MRI-based knee models. J. Biomech. 37, 1499–1504.

Ding, M., 2000. Age variations in the properties of human tibial trabecular bone and cartilage. Acta Orthop. Scandin. 71 (Suppl. 292), 1–45.

Ding, M., Hvid, I., 2000. Quantification of age-related changes in the structure model type and trabecular thickness of human tibial cancellous bone. Bone 26, 291–295.

Ding, M., Odgaard, A., Linde, F., Hvid, I., 2002. Age-related variations in the microstructure of human tibial cancellous bone. J. Orthop. Res. 20, 615–621.

Edward, I., Srivastava, M., 1989. An Introduction to Applied Geostatistics. Oxford University Press, New York, 561 p.

Fajardo, R.J., Müller, R., Ketcham, R.A., Colbert, M., 2007. Nonhuman anthropoid primate femoral neck trabecular architecture and its relationship to locomotor mode. Anat. Rec. 290, 422–436.

Fajardo, R.J., Ryan, T.M., Kappelman, J., 2002. Assessing the accuracy of high-resolution X-ray computed tomography of primate trabecular bone by comparisons with histological sections. Am. J. Phys. Anthropol. 118, 1–10.

Freeman, M., Pinskerova, V., 2005. The movement of the normal tibiofemoral joint. J. Biomech. 38, 197–208.

Galik, K., Senut, B., Pickford, M., Gommery, D., Treil, J., Kuperavage, A.J., Eckhardt, R.B., 2004. External and internal morphology of the BAR 1003′00 *Orrorin tugenensis* femur. Science 305, 1450–1453.

Gosman, J.H., Ketcham, R.A., 2008. Patterns in ontogeny of human trabecular bone from SunWatch village in the prehistoric Ohio Valley: general features of microarchitectural change. Am. J. Phys. Anthropol. 138, 318–332.

Gringarten, E., Deutsch, C.V., 2001. Variogram interpretation and modeling. Math. Geol. 33, 507–534.

Gumiaux, C., Gapais, D., Brun, J.P., 2003. Geostatistics applied to best-fit interpolation of orientation data. Technophys. 376, 241–259.

Heim, J.-L., 1982. Les hommes fossiles de La Ferrassie. Arch. Inst. Paléontol. Humaine. 38, Paris, 272 p.

Hirasaki, E., Ogihara, N., Hamada, Y., Kumakura, H., Nakatsukasa, M., 2004. Do highly trained monkeys walk like humans? A kinematic study of bipedal locomotion in bipedally trained Japanese macaques. J. Hum. Evol. 46, 739–750.

Huiskes, R., 2000. If bone is the answer, then what is the question? J. Anat. 197, 145–156.

Huiskes, R., Ruimerman, R., van Lenthe, G., Jannsen, J., 2000. Effects of mechanical forces on maintenance and adaptation of form in trabecular bone. Nature 405, 704–706.

Hunt, K.D., Cant, J.G.H., Gebo, D.L., Rose, M.D., Walker, S.E., Youlatos, D., 1996. Standardized descriptions of primate locomotor and postural modes. Primates 37, 363–387.

Hurwitz, D., Sumner, D., Andriacchi, T., Sugar, D., 1998. Dynamic knee loads during gait predict proximal tibial bone distribution. J. Biomech. 31, 423–430.

Iwaki, H., Pinskerova, V., Freeman, M., 2000. Tibio-femoral movement 1: the shapes and relative movements of the femur and tibia in the unloaded cadaver knee studied by dissection and MRI. J. Bone Joint Surg. 82-B, 1189–1195.

Jang, I.G., Kim, I.Y., 2010. Computational simulation of simultaneous cortical and trabecular bone change in human proximal femur during bone remodeling. J. Biomech. 43, 294–301.

Johal, P., Williams, A., Wragg, P., Gedroyc, W., Hunt, M., 2005. Tibio-femoral movement in the living knee. An in-vivo study of weight bearing and non-weight bearing knee kinematics using 'interventional' MRI. J. Biomech. 38, 269–276.

Kivel, T.L., Schmitt, D., 2009. Independent evolution of knuckle-walking in African apes shows that humans did not evolve from a knuckle-walking ancestor. Proc. Natl. Acad. Sci. USA 106, 14241–14246.

Komistek, R.D. (Ed.), 2005. Knee mechanics: an update of theoretical and experimental analyses. J. Biomech. 38, 195–375.

Link, T., Majumdar, S., Lin, J., Newitt, D., Augat, P., Ouyang, X., Mathur, A., Genant, H., 1998. A comparative study of trabecular bone properties in the spine and femur using high-resolution MRI and CT. J. Bone Miner. Res. 13, 122–132.

Lovejoy, C.O., 2007. The natural history of the human gait and posture. Part 3. The knee. Gait Posture 25, 325–341.

Lovejoy, C.O., Meindl, R.S., Ohman, J.C., Heiple, K.G., White, T.D., 2002. The Maka femur and its bearing on the antiquity of human walking: applying contemporary concepts of morphogenesis to the human fossil record. Am. J. Phys. Anthropol. 119, 97–133.

Macchiarelli, R., Bondioli, L., Galichon, V., Tobias, P.V., 1999. Hip bone trabecular architecture shows uniquely distinctive locomotor behaviour in South African australopithecines. J. Hum. Evol. 36, 211–232.

Macchiarelli, R., Rook, L., Bondioli, L., 2001a. Comparative analysis of the iliac trabecular architecture in extant and fossil primates by means of digital image processing techniques: implications for the reconstruction of fossil locomotor behaviours. In: de Bonis, L., Koufos, G., Andrews, P. (Eds.), Hominoid evolution and climatic change in Europe. Phylogeny of the Neogene hominoid primates of Eurasia, vol. 2. Cambridge University Press, Cambridge, pp. 60–101.

Macchiarelli, R., Nakatsukasa, M., Rook, L., Viola, T.B., Bondioli, L., 2001b. Functional adaptation of the iliac and the femoral cancellous network in a bipedal-trained Japanese macaque. Am. J. Phys. Anthropol. 99 (Suppl. 32) (abstract).

Macchiarelli, R., Mazurier, A., Volpato, V., 2007. L'apport des nouvelles technologies à l'étude des Néandertaliens. In: Vandermeersch, B., Maureille, B. (Eds.), Les Néandertaliens. Biologie et cultures. Comité des Travaux Historiques et Scientifiques, Paris, pp. 169–179.

Macchiarelli, R., Bondioli, L., Mazurier, A., 2008. Virtual dentitions: touching the hidden evidence. In: Irish, J.D., Nelson, G.C. (Eds.), Technique and application in dental anthropology. Cambridge University Press, Cambridge, pp. 426–448.

Macchiarelli, R., Mazurier, A., Illerhaus, B., Zanolli, C., 2009. *Ouranopithecus macedoniensis* (Mammalia, Primates Hominoidea): virtual reconstruction and 3D analysis of a juvenile mandibular dentition (RPl-82 and RPl-83). Geodiversitas 31, 851–864.

MacLatchy, L., Müller, R., 2002. A comparison of the femoral head and neck trabecular architecture of *Galago* and *Perodicticus* using micro-computed tomoghraphy (μCT). J. Hum. Evol. 43, 89–105.

Maga, M., Kappelman, J., Ryan, T., Ketcham, R.A., 2006. Preliminary observations on the calcaneal trabecular microarchitecture of extant large-bodied hominoids. Am. J. Phys. Anthropol. 129, 410–417.

Martin, R., Burr, D., Sharkey, N., 1998. Skeletal tissue mechanics. Springer, New York, 392 p.

Mazurier, A., 2006. Relations entre comportement locomoteur et variation cortico-trabéculaire du plateau tibial chez les Primates: analyse quantitative non-invasive à haute résolution (SR-μCT) et applications au registre fossile. PhD Thesis, Université de Poitiers, 388 p.

Mazurier, A., Macchiarelli, R., 2006. Spécificités endo-structurales du plateau tibial néandertalien. Analyse à haute-résolution du spécimen La Ferrassie 2. Bull. Mém. Soc. Anthrop. Paris 18, 233–234 (abstract).

Mazurier, A., Bondioli, L., Bravin, A., Nemoz, C., Macchiarelli, R., 2004. L'empreinte du comportement locomoteur dans l'organisation structurale fine du plateau tibial. Bull. Mém. Soc. Anthrop. Paris 16 (235) (abstract).

Mazurier, A., Bondioli, L., Bravin, A., Nemoz, C., Macchiarelli, R., 2005. High-resolution (3D SR-μCT-based) structural analysis of the primate proximal tibia: evidence for locomotion-related topographic variation. Am. J. Phys. Anthropol. 147 (Suppl. 39) (abstract).

Mazurier, A., Nakatsukasa, M., Bondioli, L., Rook, L., Macchiarelli, R., 2007. Structural signature of bipedal training in the tibial plateau of a Japanese macaque. Am. J. Phys. Anthropol. 167 (Suppl. 43) (abstract).

Mazurier, A., Volpato, V., Macchiarelli, R., 2006. Improved noninvasive microstructural analysis of fossil tissues by means of SR-microtomography. Appl. Phys. A Mat. Sc. Process 83, 229–233.

Milz, S., Putz, R., 1994. Quantitative morphology of the subchondral plate of the tibial plateau. J. Anat. 185, 103–110.

Mockenhaupt, J., Koebke, J., 1988. Densitometric analysis of the subchondral compact bone of the tibial plateau. In: Heuck, F.H.W., Keck, E. (Eds.), Fortschritte der osteologie in diagnostik und therapie. Springer-Verlag, Berlin, pp. 404–405.

Mow, V.C., Arnoczky, S.P., Jackson, D.W., 1992. Knee Meniscus: Basic and Clinical Foundations. Raven Press, New York, 204 p.

Müller-Gerbl, M., 1998. The subchondral bone plate. Adv. Anat. Embryol. Cell Biol. 141, 1–133.

Murasaki, Y., 1982. Walk! Jump! Sampei. Chikuma-shobo, Tokyo, 247 p.

Nakatsukasa, M., 2004. Acquisition of bipedalism: the Miocene hominoid record and modern analogues for bipedal protohominids. J. Anat. 204, 385–402.

Nakatsukasa, M., Hayama, S., 2003. Skeletal response to bipedalism in macaques, with emphasis on cortical bone distribution of the femur. Cour. Forsch-Inst. Sencken. 243, 35–45.
Nakatsukasa, M., Hayama, S., Preuschoft, H., 1995. Postcranial skeleton of a macaque trained for bipedal standing and walking and implications for functional adaptation. Folia Primatol. 64, 1–29.
Odgaard, A., Kabel, J., van Rietbergen, B., Dalstra, M., Huiskes, R., 1997. Fabric and elastic principal directions of cancellous bone are closely related. J. Biomech. 30, 487–495.
Ogihara, N., Makishima, H., Nakatsukasa, M., 2009. Three-dimensional musculoskeletal kinematics during bipedal locomotion in the Japanese macaque, reconstructed based on an anatomical model-matching method. J. Hum. Evol. 58, 252–261.
Ohman, J.C., Krochta, T.J., Lovejoy, C.O., Mensforth, R.P., Latimer, B., 1997. Cortical bone distribution in the femoral neck of hominoids: implications for the locomotion of *Australopithecus afarensis*. Am. J. Phys. Anthropol. 104, 117–131.
Patel, B.A., Carlson, K.J., 2007. Bone density spatial patterns in the distal radius reflect habitual hand postures adopted by quadrupedal primates. J. Hum. Evol. 52, 130–141.
Pearson, O.M., Lieberman, D.E., 2004. The aging of Wolff's "law": ontogeny and responses to mechanical loading in cortical bone. Yearb. Phys. Anthrop. 47, 63–99.
Pickford, M., Senut, B., Gommery, D., Treil, J., 2002. Bipedalism in *Orrorin tugenensis* revealed by its femora. C. R. Palevol 1, 191–203.
Pradel, A., Langer, M., Maisey, J.G., Geffard-Kuriyama, D., Cloetens, P., Janvier, P., Tafforeau, P., 2009. Skull and brain of a 300-million-year-old chimaeroid fish revealed by synchrotron holotomography. Proc. Natl. Acad. Sci. U. S. A. 106, 5224–5228.
Rafferty, K.L., 1998. Structural design of the femoral neck in primates. J. Hum. Evol. 34, 361–383.
Richmond, B.G., Nakatsukasa, M., Griffin, N.L., Ogihara, N., Ketcham, R.A., 2005. Trabecular bone structure in a bipedally trained macaque. Am. J. Phys. Anthropol. Suppl. 40, 175–176 (abstract).
Rook, L., Bondioli, L., Köhler, M., Moyà-Solà, S., Macchiarelli, R., 1999. *Oreopithecus* was a bipedal ape after all: evidence from the iliac cancellous architecture. Proc. Natl. Acad. Sci. USA 96, 8795–8799.
Ruff, C.B., 2002. Long bone articular and diaphyseal structure in Old World monkeys and apes I: locomotor effects. Am. J. Phys. Anthropol. 119, 305–342.
Ruff, C.B., Holt, B., Trinkaus, E., 2006. Who's afraid of the big bad Wolff? "Wolff's law" and bone functional adaptation. Am. J. Phys. Anthropol. 129, 484–498.
Ruimerman, R., Hilbers, P., van Rietbergen, B., Huiskes, R., 2005. A theoretical framework for strain-related trabecular bone maintenance and adaptation. J. Biomech. 38, 931–941.
Ryan, T.M., Ketcham, R.A., 2002a. The three-dimensional structure of trabecular bone in the femoral head of strepsirrhine primates. J. Hum. Evol. 43, 1–26.
Ryan, T.M., Ketcham, R.A., 2002b. Femoral head trabecular bone structure in two omomyid primates. J. Hum. Evol. 43, 241–263.
Ryan, T.M., Ketcham, R.A., 2005. Angular orientation of trabecular bone in the femoral head and its relationship to hip joint loads in leaping primates. J. Morph. 265, 249–263.
Ryan, T.M., Krovitz, G.E., 2006. Trabecular bone ontogeny in the human proximal femur. J. Hum. Evol. 51, 591–602.
Tafforeau, P., Boistel, R., Boller, E., Bravin, A., Brunet, M., Chaimanee, Y., Cloetens, P., Feist, M., Hoszowska, J., Jaeger, J.-J., Kay, R.F., Lazzari, V., Marivaux, L., Nel, A., Nemoz, C., Thibault, X., Vignaud, P., Zabler, S., 2006. Applications of X-ray synchrotron microtomography for non-destructive 3D studies of paleontological specimens. Appl. Phys. A, Mat. Sc. Process. 83, 195–202.
Tardieu, C., 1983. L'articulation du genou. Analyse morpho-fonctionelle chez les primates et les hominidés fossiles. Édition du CNRS, Paris, 108 p.
Trinkaus, E., Ruff, C.B., 1999. Diaphyseal cross-sectional geometry of Near Eastern Middle Paleolithic humans: the tibia. J. Archaeol. Sci. 26, 1289–1300.
Volpato, V., 2008. Morphogenèse de l'endostructure osseuse de l'ilion humain. C. R. Palevol. 7, 463–471.
Volpato, A., Mazurier, A., Puymerail, L., Macchiarelli, R., 2010. Spy I and II. Internal structure of the femurs and tibia. In: Semal, P., Toussaint, M. (Eds.), Spy Cave. State of 120 years of pluridisciplinary research on the Betche-aux-Rotches from Spy (Jemeppe-sur-Sambre, Province of Namur, Belgium). Institut Royal des Sciences Naturelles de Belgique, Bruxelles (in press).
Volpato, V., Viola, T.B., Nakatsukasa, M., Bondioli, L., Macchiarelli, R., 2008. Textural characteristics of the iliac-femoral trabecular pattern in a bipedally-trained Japanese macaque. Primates 49, 16–25.
Zollikofer, C.P.E., Ponce de León, M.S., 2001. Computer-assisted morphometry of hominoid fossils: the role of morphometric maps. In: de Bonis, L., Koufos, G., Andrews, P. (Eds.), Hominoid evolution and climatic change in Europe. Phylogeny of the Neogene hominoid primates of Eurasia, vol. 2. Cambridge University Press, Cambridge, pp. 50–59.